

**PREDICTION AND FAILURE ANALYSIS OF WEB
WRINKLING**

BY

JASON MITCHELL

Bachelor of Science

Oklahoma State University

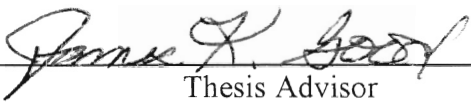
Stillwater, OK

1993

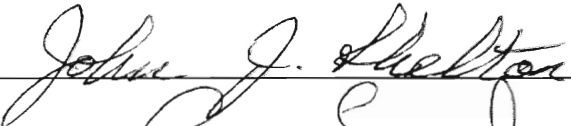
**Submitted to the faculty of the
Graduate College of the
Oklahoma State University
in partial fulfillment of
the requirements for
the Degree of
MASTER OF SCIENCE
May, 1995**


**PREDICTION AND FAILURE ANALYSIS OF WEB
WRINKLING**

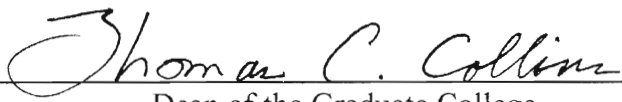
Thesis Approved:



Thesis Advisor







Dean of the Graduate College

ACKNOWLEDGMENTS

I wish to express my sincere appreciation to my major advisor, Dr. J. K. Good for his excellent leadership and creative insight. His leadership and guidance are invaluable and contribute profoundly to the beginning of my professional career. I also want to extend appreciation to Dr. C. E. Price and Dr. J. John Shelton for serving on my committee. Dr. Shelton was invaluable for his knowledge and his consulting throughout this research period.

I would like to extend many thanks and appreciation to those research fellows and friends who provided suggestions and insight to this research: Ronald Markum, Will Qualls, Nanda Vaidyanathan and Keith Ducotey.

I wish to extend my special thanks and love to my parents and family for their unbound support and patience throughout my college career and graduate research studies at Oklahoma State University.

TABLE OF CONTENTS

Chapter	Page
I. INTRODUCTION	1
II. DYNAMIC SHEAR AND WEB LATERAL DISPLACEMENT	4
Lateral Web Displacement Amplitude Ratio	4
Development of Shear Force Frequency Response	7
Shear Derivation for Web End Translation	8
Shear Derivation for Web End Rotation	10
Total Shear Derivation	12
III. STATIC WRINKLING ALGORITHM	14
Static Wrinkling Criteria	14
Critical Compressive Stress	14
Application of Critical Compressive Stress Algorithm	16
IV. EXPERIMENTAL SETUP AND PROCEDURE	23
Experimental Setup	23
Experimental Procedure	25
V. EXPERIMENTAL RESULTS	32
Analysis of Experimental Dynamic Shear	33
VI. DISCUSSION	38
Analysis of Dynamic Stress State in Web	38

Effect of Varying Stress Distribution on Critical Compressive Stress	41
Effect of Varying Stress Distribution on Traction Capacity	42
Dynamic Wrinkling Algorithm	49
Time Variance of Shear	51
 VII. CONCLUSIONS	 57
Overview	57
Future Work	58
 REFERENCES	 60

LIST OF TABLES

Table	Page
4.1 Lateral Displacement and Phase Lag Spreadsheet	28
4.2 Calculation Results From Lateral Displacement Spreadsheet	29
5.1 Static and Dynamic Critical Tram Data	35
6.1 Experimental Shear and Time Variance Data	54

LIST OF FIGURES

Figure	Page
1.1 Web Free Body Diagram and Schematic	2
2.1 Amplitude ratio and phase lag	7
2.2 Shear magnitude and phase lag	13
3.2 Web Free Body Diagram and Schematic	17
3.3 Critical Shear versus MD Stress	20
3.4 Critical Tram Error versus Critical Shear	21
3.5 MD Stress versus Critical Tram	22
4.1 Splicer Winder and Wrinkle Module	23
4.2 High Frequency Sample Plot from Lateral Displacement Spreadsheet	30
4.3 Low Frequency Sample Plot from Lateral Displacement Spreadsheet	31
5.1 Lateral Displacement and Phase Lag - Experimental Verification	33
5.2 Impending Wrinkling Tram (Dynamic/Static ratio)	36
5.3 Critical Tram - Experimental/Theory Ratio	37
6.1 Cantilevered - Pinned Beam	39
6.2 Web Stress Distribution Drawing - Dynamic Conditions	41
6.3 Traction Capacity Variance - Dynamic Conditions	47
6.4 Web Traction Capacity Versus the Load Necessary to Buckle the Web	48
6.5 Plot of Wrinkle Criteria	55

Figure	Page
6.6 Empirically Modified Wrinkle Criteria	56

NOMENCLATURE

a	web span length, (in)
b	web width, (in)
c	roller length, (in)
CMD	cross machine direction
D	web bending stiffness [$Et^3/(12-12\nu^2)$]
E	modulus of elasticity, (psi)
F	total force the web imposes onto the roller, (lb)
f_1, f_2	constants of KL given in derivations [2]
$f_{y,cr}$	internal force per unit length of the web required to cause a wrinkle
f_μ	traction capacity, (lb)
$f_{\mu,cr}$	critical traction capacity, (lb)
h_o	air film height, (in)
I	area moment of inertia [$tw^3/12$]
K	$\sqrt{T/EI}$
L	web span length, (in)
M	moment in web, (lb-in)
M_L	moment in web at $x = L$, (lb-in)
MD	machine direction

N_L	shear in web at $x = L$, (lb)
P	pressure per unit width of the web on the roller, (lb/in ³)
q	tram Error, (in)
R	roller Radius, (in)
s	web wrap distance about the Roller, (in)
t	web thickness, (in)
t_2-t_1	portion of tram period where $N_{peak} > N_{cr}$
T	web line tension, (lb _f)
V	web velocity, (fpm)
w	web width, (in)
y	lateral web displacement
y_L	lateral web displacement at $x = L$
$Y_L(s)$	lateral displacement at $x = L$, frequency domain
θ	roller wrap angle, (radians)
θ_L	tram angle $[q/c]$ for small q at $x = L$, (radians)
σ_e	normalized Stress $[\pi^2 D/w^2 t]$
σ_x	web MD Stress, (psi)
σ_y	lateral stress, (psi)
σ_2	Mohr's circle second principle stress, (psi)
$\sigma_{y,cr}$	critical compressive stress at $x = L$, (psi)
τ	web time constant $[L/V]$, (sec)
τ_{cr}	critical shear, (lb)

τ_r	roller time constant - time web is in contact with roller, (sec)
ω	tram frequency, (rad/sec)
μ	coefficient of traction
ν	dynamic viscosity of air, (lb-s/in ²)

CHAPTER I

Introduction

The research presented herein is in the area of dynamic web wrinkling. In the web handling industry, a web is considered as any material that is long and wide as compared to its thickness. Paper, foil, magnetic tape film, film, and plastic wrapping are examples of web materials. A web can withstand a high longitudinal stress prior to failure but can withstand little lateral compressive stress before buckling. The purpose of this research project is to determine how web wrinkles form as a function of web line parameters and web properties. Examples of web line parameters are web line velocity, and web tension. Examples of web properties are modulus of elasticity, Poisson's ratio, and roughness. The reason for predicting when wrinkles occur is that web degradation will occur upon wrinkling.

Wrinkling is divided into the two basic areas of static web wrinkling and dynamic web wrinkling. Static wrinkling is defined such that the tram rate of the 'steering' or tram roller is small enough so that the shear in the web is independent of the tram rate and, thus, time. Tram rate is defined as the amount of displacement, q , per unit time. Refer to

Figure 1.1 below for identification of variables. Any variables are also defined in the nomenclature.

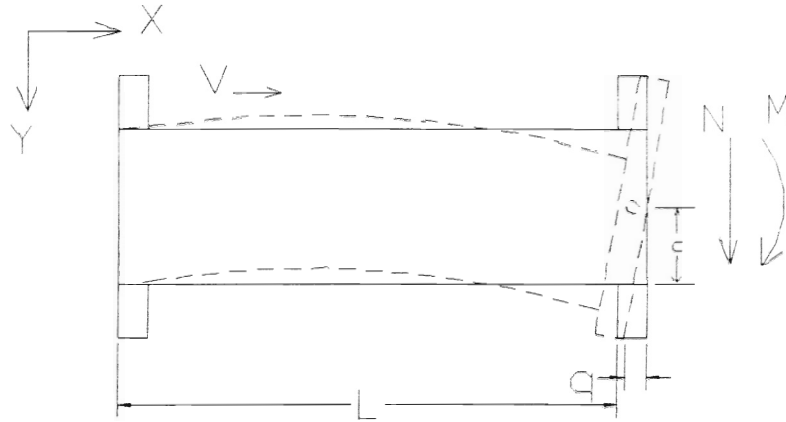


Figure 1.1 Web Free Body Diagram and Schematic

Shelton [2] developed an equation to predict the shear in a taut, planar web, for small q/c , namely:

$$N_L = \frac{T q/c}{\cosh KL - 1} \quad (1.1)$$

However, for the static case, the shear equation (1.2) accurately approximates equation (1.1) for small q/c .

$$N_L = \frac{2EI\theta}{L^2} \quad (1.2)$$

According to the shear found by equation (1.2), an accurate prediction of wrinkling is determined by relating the shear within the web, and thus tram error, with the lateral compressive stress necessary to buckle the web. This relationship is discussed in Chapter 3.

Dynamic wrinkling is defined such that the tram rate is large enough so that elementary beam theory fails in determining the shear stress because the shear is time dependent. A more detailed explanation of the differences between static wrinkling and dynamic wrinkling is made in Chapter 2.

CHAPTER II

Dynamic Shear and Web Lateral Displacement

This Chapter provides the development of dynamic shear relations for a sinusoidal input tram. The derivations apply only to center pivoted, taut, planar webs. The fundamental equations, from which Shelton [1] begins his derivation, are presented in [2]. The derivation starts with the lateral web velocity relationship for a center pivoted, taut, planar web and ends with a frequency response transfer function equating tram angular velocity with web line parameters and web material properties.

2.1 Lateral Web Displacement Amplitude Ratio

The amplitude ratio is defined as the lateral web displacement at $x = L$, y_L , divided by the span length, L , per tram angle, q/c , or $\frac{y_L/L}{q/c}$. The amplitude ratio derivation begins with the lateral web velocity relationship from “Lateral Dynamics of a Real Moving Web”, [3].

$$\frac{dy_L}{dt} = V \left[\frac{q}{c} - \theta_L \right] \quad (2.1.1)$$

Equation (2.1.2) represents the acceleration of the web for a succession of moving points on the web located at a fixed position relative to the tram roller. This equation was developed and experimentally verified by Shelton. (2.1.2) can not be obtained by differentiating (2.1.1).

$$\frac{d^2 y_L}{dt^2} = V^2 \frac{d^2 y}{dx^2} \Big|_L \quad (2.1.2)$$

From [3],

$$\frac{d^2 y}{dx^2} = \frac{1}{L} \theta_L f_2(KL) - \frac{y_L}{L^2} f_1(KL) \quad (2.1.3)$$

Where,

$$f_1(KL) = \frac{(KL)^2 (\cosh(KL) - 1)}{KL * \sinh(KL) - 2(\cosh(KL) - 1)} \quad (2.1.4)$$

and,

$$f_2(KL) = \frac{KL(KL * \cosh(KL) - \sinh(KL))}{KL * \sinh(KL) - 2(\cosh(KL) - 1)} \quad (2.1.5)$$

Substituting (2.1.1) and (2.1.2) into (2.1.3) gives:

$$\frac{1}{V^2} \frac{d^2 y_L}{dt^2} + \frac{f_2}{LV} \frac{dy_L}{dt} + \frac{f_1}{L^2} y_L = \frac{f_2}{L} \frac{q}{c} \quad (2.1.6)$$

Or,

$$\frac{L^2}{V^2} \frac{d^2 y_L}{dt^2} + \frac{Lf_2}{V} \frac{dy_L}{dt} + f_1 y_L = f_2 L \frac{q}{c} \quad (2.1.7)$$

Equation (2.1.7) is rewritten by substituting $(\frac{L}{V})$ with the time constant τ . Thus,

$$\tau^2 \frac{d^2 y_L}{dt^2} + f_2 \tau \frac{dy_L}{dt} + f_1 y_L = f_2 L \frac{q}{c} \quad (2.1.8)$$

Taking the Laplace transform of equation (2.1.8) and dividing through by f_1 gives:

$$[(\frac{1}{f_1})(\tau^2 s^2 + \frac{f_2}{f_1} \tau s + 1)]Y_L(s) = \frac{f_2}{f_1} \frac{L}{c} Q(s) \quad (2.1.9)$$

Solving for $\frac{Y_L(s) / L}{Q(s) / c}$ gives:

$$\frac{Y_L(s) / L}{Q(s) / c} = \frac{f_2 / f_1}{\frac{1}{f_1} \tau^2 s^2 + \frac{f_2}{f_1} \tau s + 1} \quad (2.1.10)$$

Equation (2.1.10) represents the lateral displacement frequency response with respect to tram angle. Illustrated below in Figure 2.1 is the frequency response and phase lag as governed by equation (2.1.10). Later in Chapter 5 experimental data is shown to confirm the theory plotted in Figure 2.1.

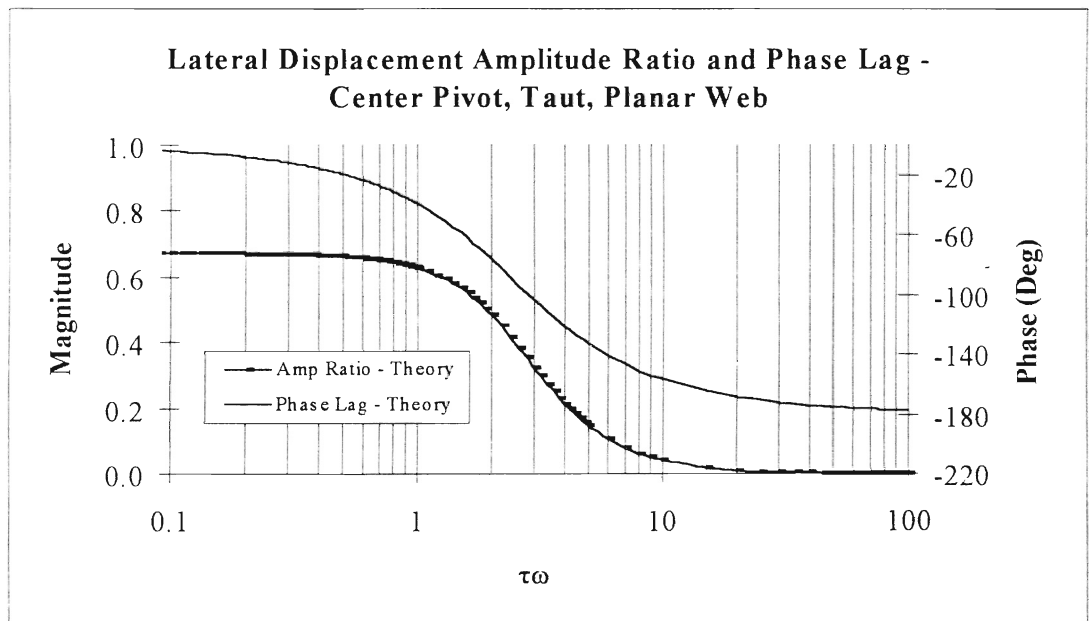


Figure 2.1 Amplitude ratio and phase lag.

2.2 Development of Shear Force Frequency Response

Another important aspect for the explanation of web behavior for the center pivoted roller is the shear magnitude. The frequency response of the shear magnitude at $x = L$, $|N_L|$, is developed in terms of the MD tension, T , displacement, q , and roller length, c . Refer to Figure 1.1 for definitions of q and c . The shear relationship is derived separately for pure rotation and pure translation of the tram roller. The two independent shear terms are then added together to obtain the total shear for a rotating and translating web. These derivations are shown below in sections 2.2.1 and 2.2.2.

2.2.1 Shear Derivation For Web End Translation

For pure translation of the downstream end of the web, where N is positive for positive y_L :

$$y''' = y_L K^3 \frac{-\sinh KL \cosh Kx + (\cosh KL - 1) \sinh Kx}{KL \sinh KL - 2(\cosh KL - 1)} \quad (2.2.1)$$

At $x = L$, substituting $y_L''' = -\frac{N_L}{EI}$.

$$\frac{N_L}{EI} = K^3 y_L \frac{\sinh KL}{KL \sinh KL - 2(\cosh KL - 1)} \quad (2.2.2)$$

Substituting $T = EIK^2$,

$$N_L = TK y_L \frac{\sinh KL}{KL \sinh KL - 2(\cosh KL - 1)} \quad (2.2.3)$$

Or solving for $\frac{N_L}{T}$ gives:

$$\frac{N_L}{T} = \frac{y_L}{L} \frac{KL \sinh KL}{KL \sinh KL - 2(\cosh KL - 1)} \quad (2.2.4)$$

Replacing $\sinh KL$ and $\cosh KL$ with a series expansion and assuming only small values of KL , equation 2.2.4 simplifies into:

$$\frac{N_L}{T} = \frac{y_L}{L} \left[\frac{12}{(KL)^2} \right] \quad (2.2.5)$$

Substituting $K = \sqrt{\frac{T}{EI}}$, and $I = \frac{1}{12} tw^3$, the translational component of shear is represented with fundamental dimensions, non-dimensional terms, and material properties as shown in equation (2.2.6).

$$\frac{N_L}{T} = \frac{y_L}{L} \left[\frac{twE}{T} \right] \left[\frac{w}{L} \right]^2 \quad (2.2.6)$$

Taking the Laplace transform of equation (2.2.5) results in the translational shear frequency response.

$$\left. \frac{N(s)_L / T}{Q(s) / c} \right|_{Trans} = \frac{Y_L(s) / L}{Q(s) / c} \left[\frac{12}{(KL)^2} \right] \quad (2.2.7)$$

Where $\frac{Y_L(s)/L}{Q(s)/c}$ is defined by equation (2.1.10).

2.2.2 Shear Derivation For Web End Rotation

For pure rotation of the end of the web, where N is negative for positive y'_L :

$$y''' = K^2 \theta_L \frac{(\cosh KL - 1) \cosh Kx + (KL - \sinh KL) \sinh Kx}{KL \sinh KL - 2(\cosh KL - 1)} \quad (2.2.8)$$

at $x = L$ substituting $y'''_L = \frac{-N_L}{EI}$,

$$\frac{N_L}{EI} = K^2 \theta_L \frac{\sinh^2 KL - \cosh^2 KL + \cosh KL - KL \sinh KL}{KL \sinh KL - 2(\cosh KL - 1)} \quad (2.2.9)$$

Substituting $EIK^2 = T$ into equation (2.2.9) gives:

$$N_L = \frac{KL \sinh KL - (\cosh KL - 1)}{KL \sinh KL - 2(\cosh KL - 1)} T \quad (2.2.10)$$

Or, dividing through by T , equation (2.2.10) is rewritten as:

$$\frac{N_L}{T} = -\theta_L \frac{KL \sinh KL - (\cosh KL - 1)}{KL \sinh KL - 2(\cosh KL - 1)} \quad (2.2.11)$$

Applying a series expansion for $\sinh KL$ and $\cosh KL$ and assuming only small values of KL , equation (2.2.11) simplifies into:

$$\frac{N_L}{T} = -\theta_L \left[\frac{6}{(KL)^2} \right] \quad (2.2.12)$$

Again, substituting $K = \sqrt{\frac{T}{EI}}$, and $I = \frac{1}{12} tw^3$, the shear force due only to rotation is represented with fundamental dimensions, non-dimensional terms, and material properties as shown in equation (2.2.13).

$$\frac{N_L}{T} = -\theta_L \left[\frac{twE}{2T} \right] \left[\frac{w}{L} \right]^2 \quad (2.2.13)$$

Taking the Laplace transform of equation (2.2.12) results in the shear frequency response due to a pure web rotation at $x = L$.

$$\left. \frac{N_L / T}{Q(s) / c} \right|_{Rot} = \frac{Y_L(s) / L}{Q(s) / c} \left[\frac{6}{(KL)^2} \right] \quad (2.2.14)$$

Where $\frac{Y_L(s) / L}{Q(s) / c}$ is defined by equation (2.1.10).

2.2.3 Total Shear Derivation

Summing the rotational and translational component of shear and simplifying for small KL gives the total shear magnitude frequency response.

$$\left. \frac{N_L / T}{Q(s) / c} \right|_{\text{Total}} = \left. \frac{N_L / T}{Q(s) / c} \right|_{\text{Rot}} + \left. \frac{N_L / T}{Q(s) / c} \right|_{\text{Trans}} \quad (2.2.15)$$

Substituting equations (2.2.14) and (2.2.7) into (2.2.15) and algebraically simplifying results in the total shear frequency response equation.

$$\left. \frac{N_L / T}{Q(s) / c} \right|_{\text{Total}} = \frac{2 - \tau^2 s^2}{(KL)^2 \left[\frac{1}{6} \tau^2 s^2 + \frac{2}{3} \tau s + 1 \right]} \quad (2.2.16)$$

Illustrated below in Figure 2.2 is the theoretical dynamic shear magnitude and phase lag as predicted by equation (2.2.16).

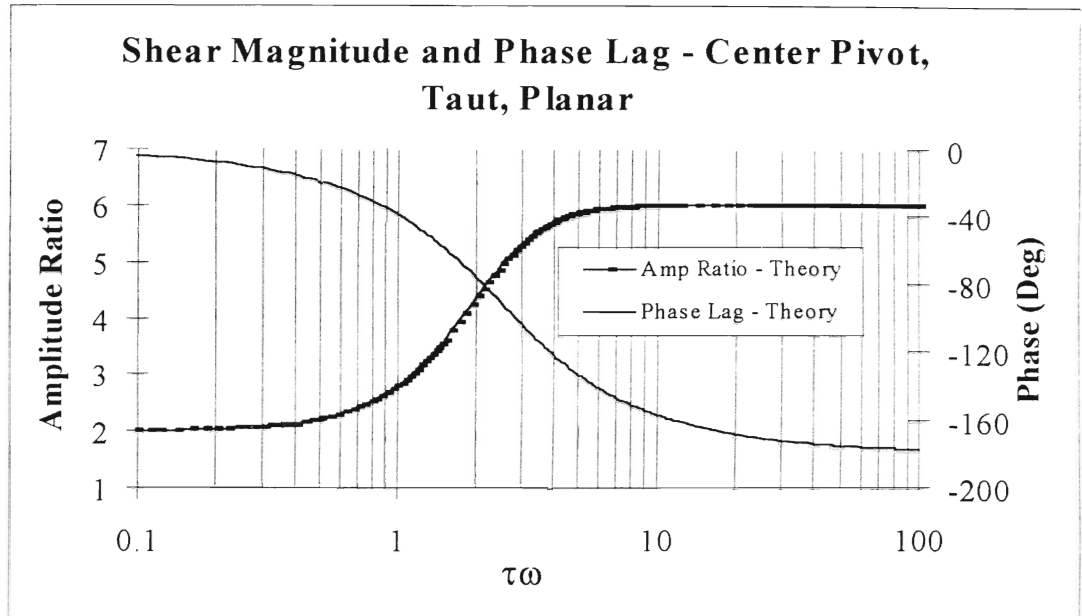


Figure 2.2 Shear Magnitude and Phase Lag - Center Pivot, Taut, Planar Web

As seen from Figure 2.2, the peak dynamic shear magnitude at high $\tau\omega$ is three times the static shear magnitude at low $\tau\omega$. It is important to note that the shear magnitude for high $\tau\omega$ is accurately represented with the equation $N_L = \frac{6EI\theta}{L^2}$, whereas the equation for static shear is $N_L = \frac{2EI\theta}{L^2}$, which is a factor of 3 smaller for the same rotation angle, θ . Also, the shear magnitude approaches 180 degrees out of phase with the displacement at high $\tau\omega$. Conversely, the shear is in phase with the displacement for static cases or low $\tau\omega$ values.

CHAPTER III

Static Wrinkling Algorithm

3.1 Static Wrinkling Criteria

In this Chapter the static wrinkling algorithm developed by Good et al [7] and Quan [4] is derived for a center pivoted, taut, planar web. The wrinkle algorithm is applicable for the static shear and regime I cases, and used to determine the tram error incident upon web failure, where regime I is independent of roller traction. A main assumption for regime I is that no slippage appears between the web and roller. The wrinkling algorithm is used to calculate the critical shear and critical buckling stress. When the critical shear and critical buckling stress are known, the critical tram error is calculated in terms of web line parameters and web material properties.

3.1.1 Critical Compressive Stress

Good [7] produced a static algorithm that determines the shear stress necessary to buckle the web. This algorithm was developed on the assumption that troughs oriented in

the machine direction have a half sinusoid cross section shape. The algorithm was later modified on the assumption that the troughs do not have a perfect sinusoid cross section but rather flatten out into a troughed shape over the majority of the length. Quan [4] derived expressions for the critical CMD stress for both the sinusoid cross section and the troughed cross section. Both expressions require calculating the half wave number, n , and other constants which are dependent on wrap angle, material properties, and web dimensions.

For the method assuming a sinusoid web cross section used to calculate $\sigma_{y,cr}$, the half wave number is determined by solving the inequality shown in equation (3.1) below. Calculating $\sigma_{y,cr}$ with the sinusoid cross section assumption gives nearly identical results as the troughed cross section method

$$\sigma_e \left[1 - n^2 (n-1)^2 \frac{a^4}{b^4} \right] > \sigma_x > \sigma_e \left[1 + n^2 (n+1)^2 \frac{a^4}{b^4} \right] \quad (3.1)$$

The lateral compressive stress necessary to buckle the web is now calculated with equation (3.2).

$$\sigma_{y,cr} = \frac{b^2}{n^2 a^2} \left[\sigma_e \left(1 + \frac{n^2 a^2}{b^2} \right)^2 - \sigma_x \right] \quad (3.2)$$

Equations (3.1) and (3.2) supply us with an accurate failure prediction model for critical compressive stress.

3.1.2 Application of Critical Compressive Stress Algorithm

Now that an expression for the critical compressive stress is available, we can incorporate it into a failure algorithm in terms of web line properties and material properties. First, Mohr's circle analysis is applied to relate the compressive stress with the shear stress, compressive stress, and tensile stress. The following equation gives the Mohr's circle relationship for these stresses.

$$\sigma_2 = \frac{\sigma_x + \sigma_y}{2} - \sqrt{\left(\frac{\sigma_x - \sigma_y}{2}\right)^2 + \tau^2} \quad (3.3)$$

Where τ is the shear stress in equation (3.3). With equation (3.3) the maximum allowable shear stress is determined by substituting $\sigma_{y,cr}$, calculated with equation (3.2) for σ_2 yielding equation (3.4).

$$\tau_{cr} = \sqrt{\sigma_{y,cr}^2 - \sigma_x \sigma_{y,cr}} \quad (3.4)$$

To relate the critical shear stress with web line parameters, web properties, and tram error, web beam analysis is performed. The following schematic and web free body diagram illustrated below is used as a reference for beam analysis.

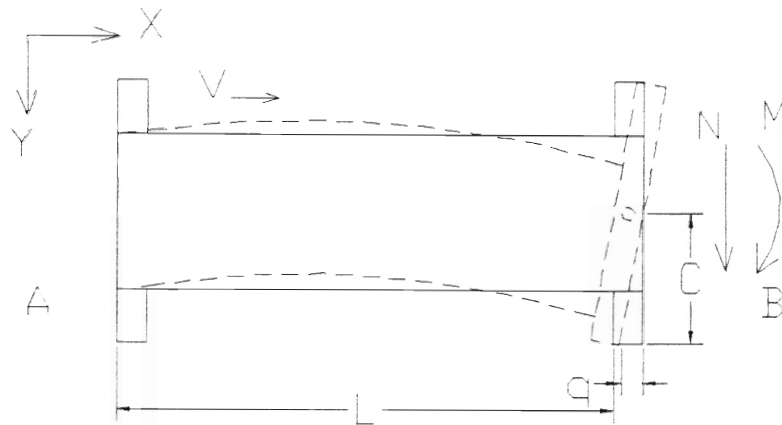


Figure 3.2 Drawing of Web Free Body Diagram and Schematic.

The moment in the beam is:

$$M_{AB} = N * x - M \quad (3.5)$$

With this moment equation you can express the beam angle (q/c), in terms of the moment by employing Castigliano's second theorem:

$$\theta_A = \frac{\partial U}{\partial M} = \int_L \frac{M_{AB}}{EI} \frac{\partial M_{AB}}{\partial M} dx = \frac{FL^2}{2EI} \quad (3.6)$$

Similarly, at the critical condition:

$$\theta_{A\sigma} = \frac{FL^2}{2EI} \approx \frac{6\tau_\sigma L^2}{Ew^2} \quad (3.7)$$

Finally, for small tram angles, equation (3.7) is accurately approximated as:

$$\frac{\text{TRAM ERROR}}{L_R} = \frac{6\tau_{cr}L^2}{Ew^2} \quad (3.8)$$

This failure criterion is only valid for a center pivoted roller in static shear conditions and regime I cases. Equation (3.8) allows one to compare the critical tram error with web line parameters and web material properties. The failure algorithm for an end pivoted roller is the same as the center pivoted roller algorithm as long as (1) L_R is measured from the point of rotation and (2) the tram error of the end-pivoted roller does not alter the web line tension.

Equation (3.8) is an accurate model for web failure prediction, however it requires the iterative process of calculating the half wave number, n , which in turn is used to calculate the critical compressive stress and then the critical shear stress. To simplify calculations of the critical shear and lateral compressive stress, another approach is documented by Shelton [5]. Timoshenko and Gere [6] developed an analysis of buckling of a rectangular plate with tension in the machine direction, tension in the cross machine or lateral direction, and simple supports at all edges. The assumptions made while simplifying a plate to a web are that Poisson's ratio is 0.3, and the longitudinal strain, (σ_x/E) , is much larger than (t/L) and $(t/L)^3(E/\sigma_x)^{0.5}$. These are safe assumptions when dealing with most common web products. The simplified equation for critical buckling stress is:

$$\sigma_{y,cr} = -1.9E \frac{t}{L} \sqrt{\frac{\sigma_x}{E}} \quad (3.9)$$

Substituting equation (3.9) into equation (3.7) yields a simplified expression for the critical shear stress as shown in equation (3.10).

$$\tau_{cr} = \sqrt{3.61 \left(\frac{t}{L} \right)^2 \sigma_x E + 1.9 \sigma_x E \frac{t}{L} \sqrt{\frac{\sigma_x}{E}}} \quad (3.10)$$

The shear force is defined as $N = \tau w$. Similarly, the critical shear force is defined as $N_{cr} = \tau_{cr} tw$. Multiplying equation (3.10) by tw gives the critical shear equation in terms of the MD stress and fundamental web parameters t , L , and E as shown in equation (3.11).

$$N_{cr} = tw \sqrt{3.61 \left(\frac{t}{L} \right)^2 \sigma_x E + 1.9 \sigma_x E \frac{t}{L} \sqrt{\frac{\sigma_x}{E}}} \quad (3.11)$$

For a more practical application of the failure criteria, substitute equation (3.4) into equation (3.10) and obtain an expression for critical shear stress in terms of the fundamental web parameters and web material properties. This relationship is shown in the condensed form in equation (3.12).

$$TE = \frac{L^2 tw(L_R)}{2EI} (\sigma_{y,cr}^2 - \sigma_x \sigma_{y,cr}) \quad (3.12)$$

Equation (3.12) is the experimentally verified failure criteria for a center pivoted or end pivoted, taut, planar web in terms of web line properties and web material properties. This static wrinkling criteria is used in a spreadsheet to confirm static wrinkling tests on the wrinkle module.

Illustrated below are three charts that compare how the MD stress varies with critical shear, tram error varies with critical shear, and how the MD stress varies with critical tram error as governed by equations (3.11), (3.13), and (3.14). The following charts apply strictly to Regime I, static shear wrinkles.

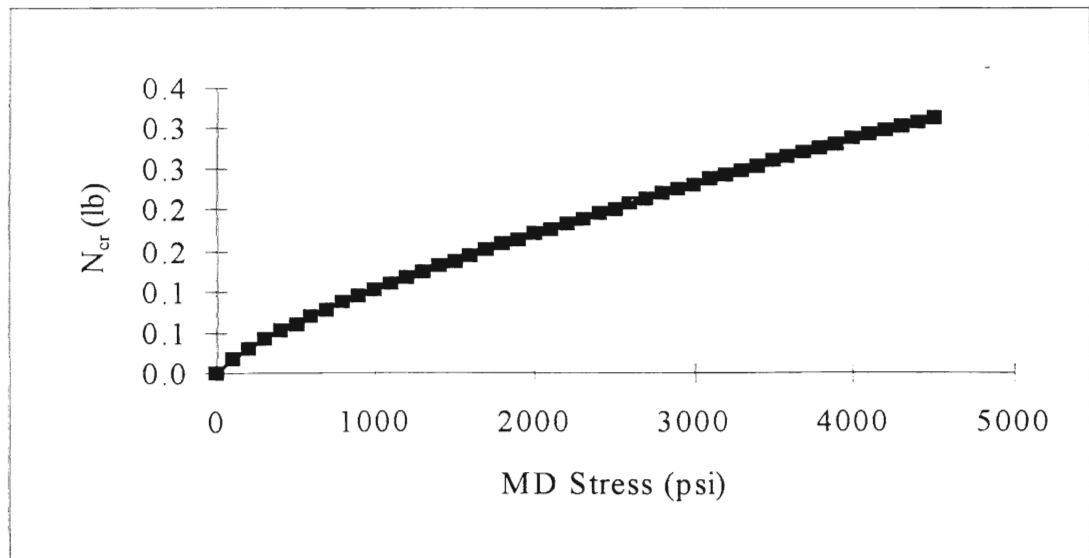


Figure 3.3 Critical Shear versus MD Stress - I377, 48 Gage, Static Wrinkling

Figure 3.3 illustrates the affect of MD stress upon the static shear required to wrinkle a 48 gage, ICI 377, PET web as governed by equation (3.10). This relation is valid for any isotropic material with constant cross section and unchanging material properties.

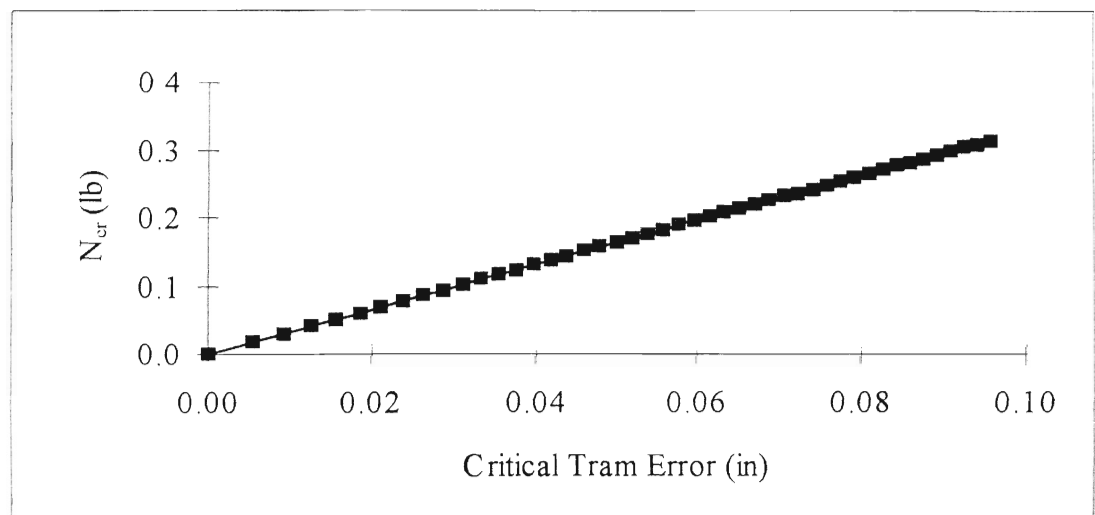


Figure 3.4 Critical Tram Error versus Critical Shear - I377, 48 Gage, Static Wrinkling

Figure 3.4 illustrates how the critical tram error varies almost linearly with the critical shear for any isotropic material with a constant cross section per equation (3.10).

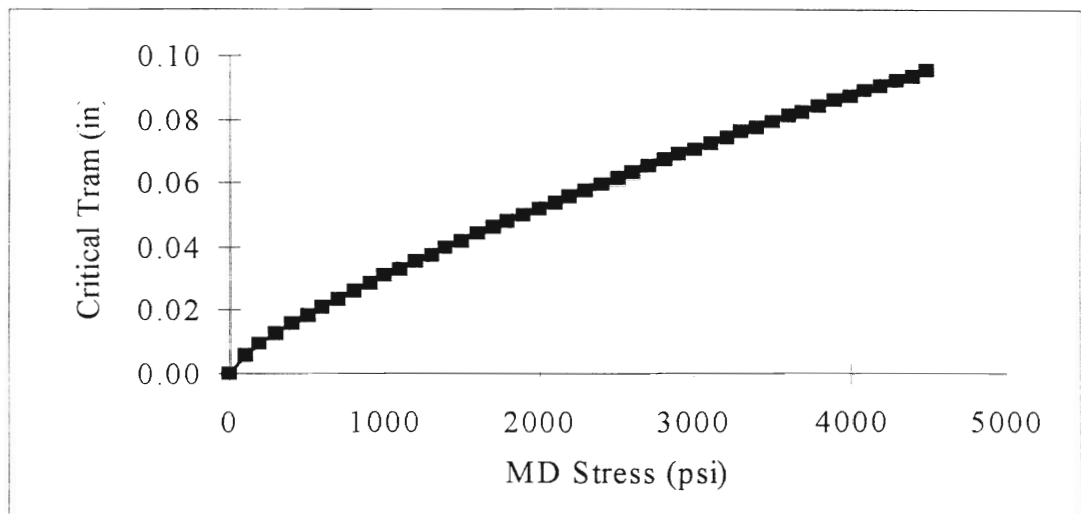


Figure 3.5 MD Stress versus Critical Tram - I377, 48 Gage, Static Wrinkling

Figure 3.5 illustrates that the MD stress required to wrinkle the web varies non-linearly with the resulting critical tram. This chart is important because it shows that increasing the MD stress, and thus the MD tension, requires an increase in tram to wrinkle the web. However, increasing the tension may cause other problems within the web line process.

CHAPTER IV

Experimental Setup and Procedure

4.1 Experimental Setup

Web wrinkling experiments for static and dynamic tram conditions were performed at the Web Handling Research Center at OSU. The entire test apparatus used to conduct these experiments is shown below in Figure 4.1.

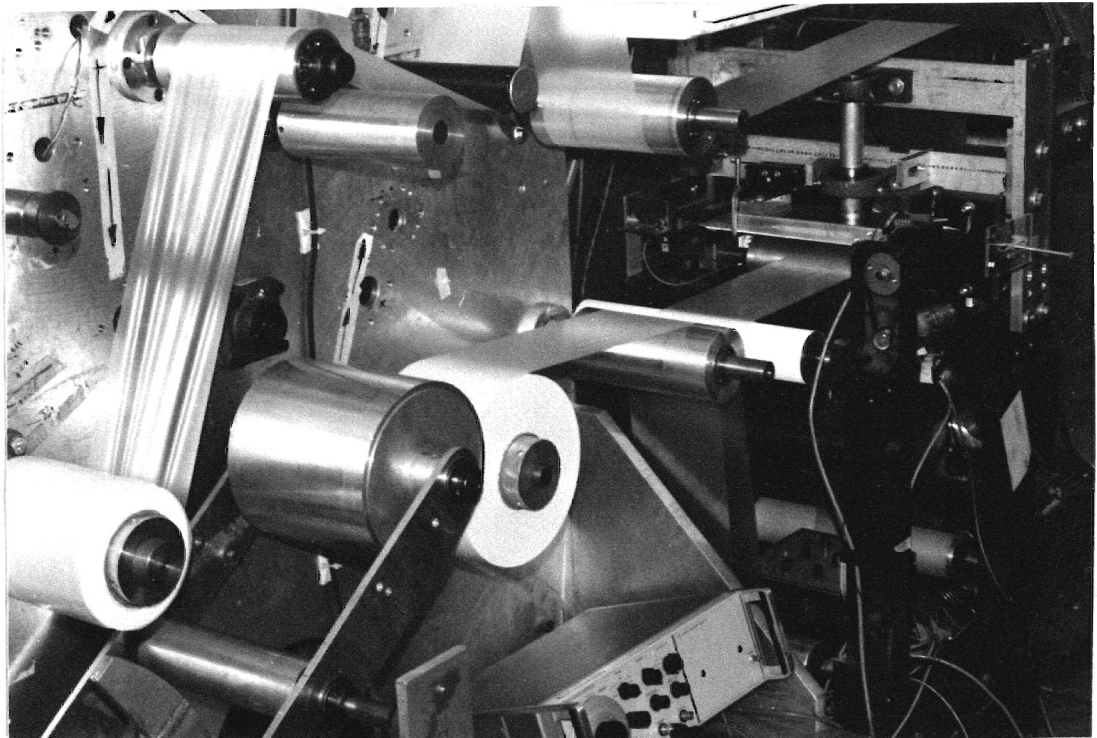


Figure 4.1 Splicer winder with wrinkle module.

The wrinkle module shown in Figure 4.1, donated by 3M, was originally built for an end pivot tram roller. However, the wrinkle module was modified for a center pivoted tram roller. Previous wrinkling research, primarily static wrinkling, was experimentally verified with an end pivoting tram roller. In the previous research in static wrinkling, a micrometer was used to impose a known displacement to the tram roller [4]. Very slowly imposing a known tram displacement simulates the low $\tau\omega$ shear magnitude and displacement magnitude web response. The experimental apparatus was later modified for a center pivoted tram roller. Center pivoting ensures symmetrical geometry when comparing CW tram rotation with CCW tram rotation, whereas with end pivoting the stress distribution changes when comparing CW rotation with CCW rotation. In other words, for an end pivoted roller at high frequency conditions, there would be an oscillating bending stress superimposed upon an oscillating uniform stress.

To control the tram displacement and frequency, a servo motor was mounted to the experimental apparatus. A function generator was used to input a sinusoidal voltage to the servo motor to produce a sinusoidal tram input displacement. Adjusting the amplitude and frequency of the tram roller was easily accomplished by adjusting the amplitude and frequency of the output voltage from the function generator.

To perform successful wrinkling experiments, small wrinkles must be spotted as well as bigger wrinkles. To account for poor lighting surrounding the tram roller, a laser was mounted on the edge of the roller mount such that the light beam skims across the

tram roller. When the web wrinkles as it crosses the tram roller, the light beam illuminates the wrinkled web material allowing visual contact of the wrinkle.

4.2 Experimental Procedure

The first step taken when performing experiments is to warm-up all the electronics for at least 20 minutes. This equipment includes:

- 1) Splicer winder motor and load cell.
- 2) Fife (SE-4) displacement transducers.
- 3) Fife A9 signal processor feedback.
- 4) Servo motor.
- 5) DCDT displacement transducer.
- 6) Data acquisition board.

Warm-up of this equipment ensures that electronic drift is minimized when taking data, resulting in better data. After the equipment is sufficiently warmed, the load cell on the splicer winder must be calibrated. This is done by feeding a string through the web path and hanging a known weight from the end of the string and adjusting the tension control until the tension scale reads the proper weight. Now that the load cell is calibrated the tram roller must be adjusted so it is parallel with the upstream roller. This is done with low web velocity and under low $\tau\omega$ or static conditions so as to avoid air entrainment or

any time variance problems of shear, respectively. The tram roller position is adjusted by tweaking the null position on the A9 signal processor until a static wrinkle appears during full servo motor extension and retraction. Note that the tram is still under a sinusoidal motion. Next, the data acquisition is prepared for use. When the proper channels are connected, a sample output run is printed to the screen and viewed to ensure all channels and input data appear normal. When all instruments are warm and are working properly, then experiments are run and recorded using a 80386 computer and Labtech Notebook data acquisition software.

There were several precautions taken while performing wrinkling experiments. These primarily come from the necessity to operate in Regime I wrinkling, because the theory developed in Chapter 2 fails when traction is lost between the web and tram roller. To ensure sufficient traction is present, low web velocities are run in conjunction with high web tension. Low web velocity combined with high tension produce a minimum amount of air entrainment, thus keeping the coefficient of traction at a maximum value. High web tension also increases the normal pressure applied on the rollers, thus increasing the traction capacity of the web.

Experimentally, the first step taken was to confirm the frequency response shear magnitude, amplitude ratio, and phase lag equations as shown in Chapter 2. Data read into the computer included the lateral web displacement relative to the tram roller, and the tram displacement via the DCDT. Data was taken for values of $\tau\omega$ varying from 0.4 to 12. These values represent practical limits of $\tau\omega$. With the equipment used in this research, specifically the lateral web displacement Fife (SE-4) transducer, the upper end of

$\tau\omega$ was limited to 12 because the lateral web displacement approaches zero with increasing $\tau\omega$, and the resolution of the Fife (SE-4) transducer is not sufficient to accurately read such low displacements. Many data points were taken at varying values of $\tau\omega$ and the resulting data were imported into an Excel spreadsheet for data analysis. All of the experiments were performed with 48 gage ICI 377 polyester.

The resolution of the Fife transducer is 0.002 in. However, the web edge has slight discontinuities, decreasing the effective resolution of the Fife transducer to approximately 0.005 in. This resolution is sufficient for lateral web displacements of no less than 0.020 in., which is sufficient for all $\tau\omega$ values up to 12. The DCDT resolution is 0.001 in., which results in very accurate experimental tram data.

In the lateral displacement and phase lag spreadsheet, Microsoft Excel Solver is used to fit a theoretical sine wave to the output of the DCDT. This theoretical sine wave was, in turn, used to determine the tram frequency, amplitude, and period. The tram frequency, amplitude, and period are used to calculate experimental values of $\tau\omega$, shear magnitude, amplitude ratio, and phase lag. These experimental values are then plotted on top of theoretical predictions from equations (2.1.10) and (2.2.16) for comparison and analysis. A sample lateral displacement and phase lag spreadsheet is shown below. Also, experimental verification of amplitude ratio and phase lag is illustrated later in Chapter 5.

Form: $\text{Asin}(Bt/2\pi + D) +$							
			Tram:		Minimize		
Amp.			0.0415		Tram:		
Per.			10.2319		0.2011		
D.C off.			0.2934				
Phase			5.1985				
Time	Web disp	(in)	Avg. Web Disp. (in)	Tram Err (V)	(in)	Theoretical Sine wave: Tram:	Difference:
0	4.2871	0.311		0.3296	0.253	0.2567	0.0032
0.2	4.27	0.302	0.3066	0.3149	0.256	0.2594	0.0038
0.4	4.2358	0.286	0.2941	0.2905	0.259	0.2625	0.0035
0.6	4.2261	0.281	0.2834	0.2612	0.263	0.2662	0.0030
0.8	4.2432	0.289	0.2852	0.2271	0.268	0.2702	0.0022
1	4.248	0.292	0.2906	0.1904	0.273	0.2746	0.0015
1.2	4.2578	0.297	0.2941	0.1514	0.279	0.2793	0.0006
1.4	4.2676	0.301	0.2989	0.1123	0.284	0.2842	0.0000
1.6	4.2798	0.307	0.3043	0.0732	0.290	0.2892	0.0005
1.8	4.2676	0.301	0.3043	0.0342	0.295	0.2943	0.0009
2	4.2627	0.299	0.3001	-0.0049	0.301	0.2993	0.0013
2.2	4.2578	0.297	0.2977	-0.0439	0.306	0.3043	0.0019
2.4	4.2773	0.306	0.3013	-0.0806	0.311	0.3092	0.0022
2.6	4.2944	0.314	0.3102	-0.1123	0.316	0.3137	0.0021
2.8	4.2749	0.305	0.3096	-0.144	0.320	0.3180	0.0023
3	4.3042	0.319	0.3120	-0.166	0.323	0.3219	0.0015
3.2	4.3408	0.337	0.3281	-0.1929	0.327	0.3254	0.0018
3.4	4.3359	0.335	0.3358	-0.21	0.330	0.3284	0.0012
3.6	4.3408	0.337	0.3358	-0.2222	0.331	0.3309	0.0005
3.8	4.3481	0.341	0.3388	-0.2295	0.332	0.3328	0.0004
4	4.3604	0.347	0.3436	-0.2344	0.333	0.3341	0.0010
4.2	4.375	0.354	0.3501	-0.2368	0.333	0.3348	0.0014
4.4	4.397	0.364	0.3591	-0.2368	0.333	0.3349	0.0015
4.6	4.3994	0.366	0.3650	-0.2344	0.333	0.3343	0.0012
4.8	4.4141	0.373	0.3692	-0.2344	0.333	0.3332	0.0001
5	4.4336	0.382	0.3775	-0.2271	0.332	0.3314	0.0007
5.2	4.4214	0.376	0.3793	-0.2026	0.329	0.3291	0.0005
5.4	4.4287	0.380	0.3781	-0.1831	0.326	0.3262	0.0003
5.6	4.4482	0.389	0.3846	-0.1587	0.322	0.3228	0.0004
5.8	4.4287	0.380	0.3846	-0.1318	0.319	0.3190	0.0004
6	4.4458	0.388	0.3840	-0.105	0.315	0.3148	0.0000
6.2	4.4751	0.403	0.3954	-0.0708	0.310	0.3103	0.0003
6.4	4.4556	0.393	0.3978	-0.0391	0.306	0.3055	0.0000
6.6	4.4751	0.403	0.3978	-0.0049	0.301	0.3006	0.0001
6.8	4.4751	0.403	0.4025	0.0293	0.296	0.2955	0.0004
7	4.4458	0.388	0.3954	0.0635	0.291	0.2904	0.0006
7.2	4.4702	0.400	0.3942	0.0977	0.286	0.2854	0.0008
7.4	4.4556	0.393	0.3966	0.1318	0.281	0.2804	0.0010
7.6	4.436	0.383	0.3882	0.166	0.277	0.2757	0.0009
7.8	4.4238	0.377	0.3805	0.1953	0.272	0.2712	0.0012
8	4.4263	0.379	0.3781	0.2246	0.268	0.2671	0.0012

Table 4.1 Lateral Displacement and Phase Lag Spreadsheet

48 gage					
qo74359.xls			T (lb.)	Q (in.)	C (in.)
Exp. Amplitude Ratio			9	0.0412	9.75
Max Avg.	Min Avg.	P-P			
Web disp	Web disp	Amplitude	t(in)	w(in)	Theta (at L)
0.0000	0.0000	0.0000	0.00048	6	0.004222
Max Tram	Min Tram	P-P Tram	L(in)	I = 1/12(b*h^3)	
	Amplitude		18	0.00864	
0.3334	0.2511	0.0823			
Exp. Amplitude Ratio -			K = Sqrt(T/EI)		KL =
0.000			4.167E-02		0.75
Experimental Phase Lag			{N(at L)/T / Q/C } * (KL)^2 (chart) =		
Tram To Web To			3.31		
0 0			N (at L) = 0.22		
Tram Frequency(rad/s)			Using N (at L) = 2EI*Theta/L^2		
0.61			N (at L)= 0.14		
Exp. Phase Lag (Deg)			f1 = 6.0560254		
0			f2 = 4.07445405		
Web Velocity (FPM)			f2/f1 = 0.67279342		
Tau * Omega			q (dynamic) / q (static)		
Theoretical Amplitude Ratio			Theory	Experimental	
0.592			0.60	0.63	
Theoretical Phase Lag					
-51.1					

Table 4.2 Calculation Results From Lateral Displacement Spreadsheet

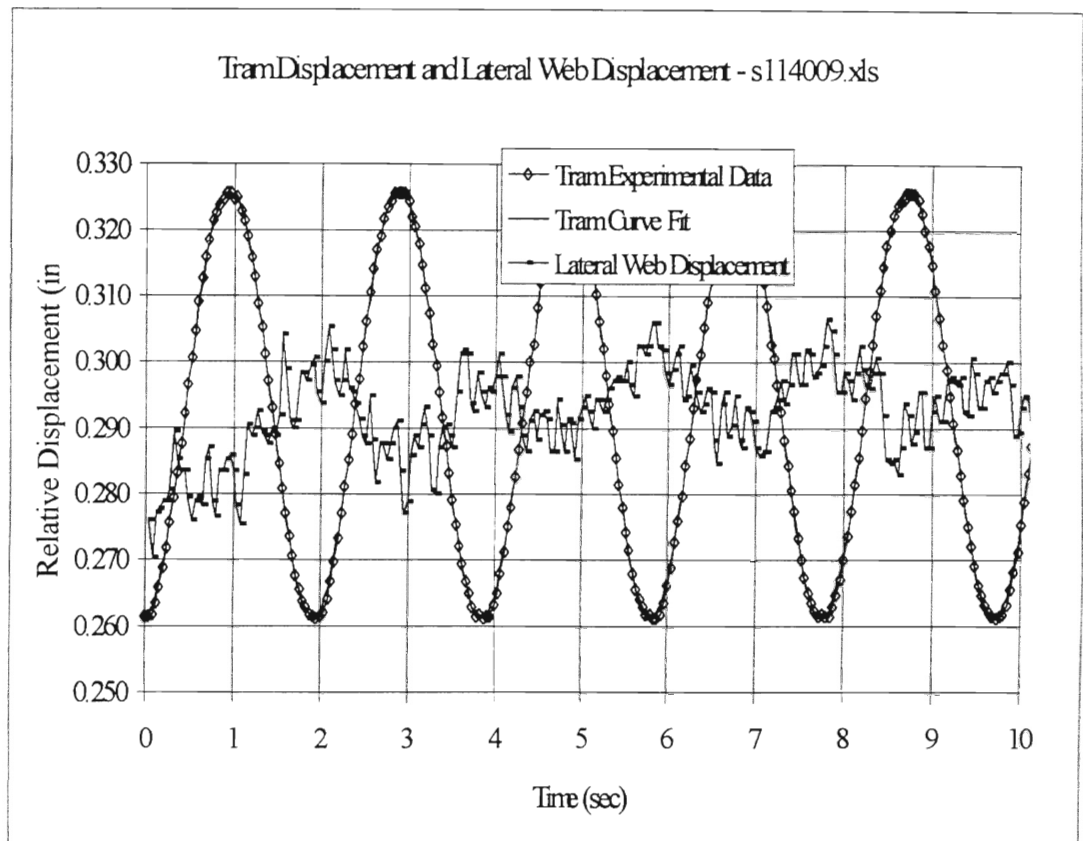


Figure 4.2 High Frequency Sample Plot From Lateral Displacement Spreadsheet

Figure 4.2 represents a high frequency, $\tau\omega = 7.5$, experimental data chart. It includes the tram experimental data, corresponding tram curve fit and resulting lateral web displacement. Note that the web displacement is relatively small as compared to the tram displacement and that the web displacement phase lag is nearly 180 degrees from the tram displacement.

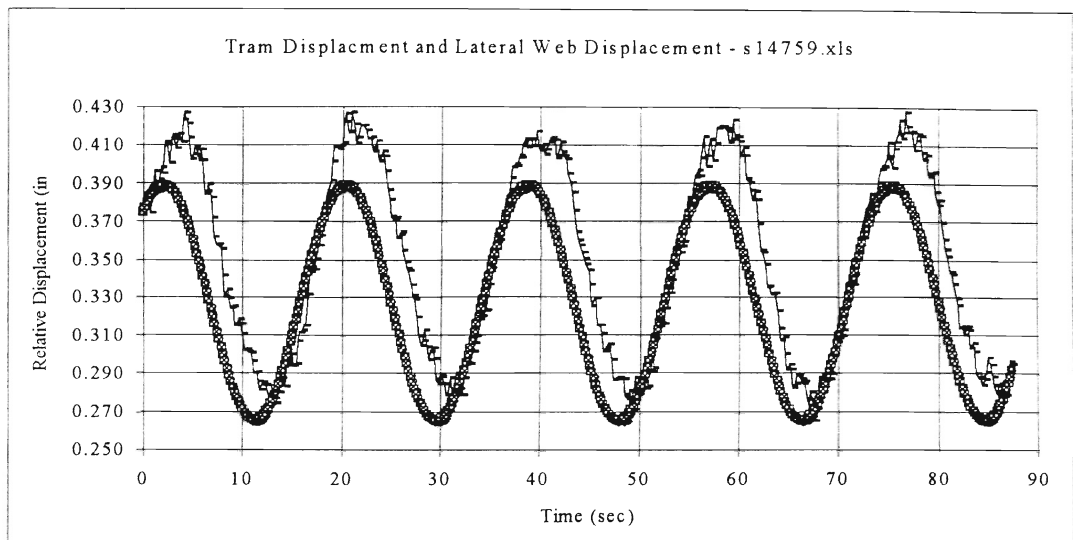


Figure 4.3 Low Frequency Sample Plot from Lateral Displacement Spreadsheet

Figure 4.3 represents a low frequency, $\tau\omega = 0.43$, experimental data chart. This chart illustrates that the web displacement grows relatively larger than the tram and the tram phase lag approaches zero. This is common among low frequency web response experimental data.

CHAPTER V

Experimental results

After performing many experiments at varying values of $\tau\omega$, the amplitude ratio and phase lag results attained from the spreadsheet in Table 4.2 are plotted over theoretical predictions, as shown below in Figure 5.1. This chart shows the experimental verification of equation (2.1.10). Verification of equation (2.1.10), in turn, leads to confidence that the shear magnitude, described by equation (2.2.16), does exist within the web. Confidence that the shear magnitude described by equation (2.2.16) exists within the web leads to the development of the dynamic wrinkling criteria as developed in Chapter 3.

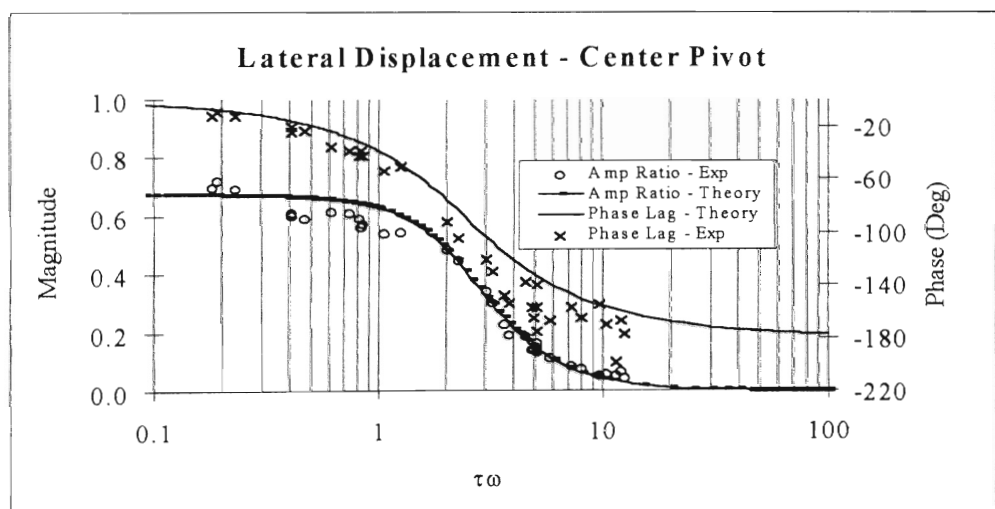


Figure 5.1 Lateral Displacement and Phase Lag - Experimental Verification

With the web amplitude ratio and phase lag relations verified, as governed by equation (2.1.10), dynamic wrinkling experiments are performed next to begin development of a working wrinkling algorithm.

5.1 Analysis of experimental dynamic shear

To develop a wrinkling algorithm which describes when a web will wrinkle under dynamic conditions, we must understand how a web acts while subject to dynamic shear. While referring to Figure 2.2, note that, for increasing $\tau\omega$, dynamic shear grows larger than static shear by a magnitude of 3. The first obvious conclusion that someone may make is that the web will wrinkle at a tram angle inversely proportional to the shear increase. For example, for any given $\tau\omega$, if the critical shear is two times that created by static conditions, one might expect the critical tram angle to be one half of the critical tram angle for the static condition. Similarly, for large $\tau\omega$, the shear force is three times the shear force created by static conditions; therefore, we expect the dynamic critical angle to be one third of the critical angle resulting from static conditions. If this was true, then we could modify the static wrinkling algorithm by substituting the dynamic shear equation, equation (2.2.16), for the static shear equation into the static wrinkling algorithm, and the problem is solved. However, observing experimental data, given in Figure 5.2 below, shows that the critical tram increasingly drifts from theoretical prediction with increasing $\tau\omega$. Note that low $\tau\omega$ experiments merge with theoretical predictions. This shows that the

verified static wrinkling tests correspond with a low $\tau\omega$ frequency response. Note that both Figures 5.2 and 5.3 could have been presented as ratios of shear without affecting the graphs.

	{1}	{2}	
	Q(large $\tau\omega$)/Q(low $\tau\omega$)		
$\tau\omega$	Theory [eqn. (2.2.16)] / [eqn. (1.2)]	Experimental	{2} / {1}
0.43	0.93	0.99	1.06
0.61	0.86	0.9	1.05
0.72	0.82	0.87	1.06
0.78	0.8	0.85	1.06
0.8	0.79	0.88	1.11
0.84	0.77	0.82	1.06
0.95	0.73	0.74	1.01
0.96	0.73	0.76	1.04
1.03	0.7	0.75	1.07
1.2	0.64	0.69	1.08
1.32	0.6	0.63	1.05
1.44	0.57	0.58	1.02
1.55	0.54	0.66	1.22
1.61	0.53	0.57	1.08
1.88	0.48	0.52	1.08
1.97	0.46	0.54	1.17
2.02	0.45	0.54	1.20
2.03	0.45	0.48	1.07
2.18	0.43	0.51	1.19
2.57	0.4	0.46	1.15
2.6	0.4	0.51	1.28
2.75	0.39	0.5	1.28
3.37	0.36	0.46	1.28
3.53	0.36	0.5	1.39
3.64	0.36	0.51	1.42
4	0.35	0.44	1.26
4.09	0.35	0.64	1.83
4.96	0.34	0.5	1.47
5.07	0.34	0.54	1.59
5.2	0.34	0.6	1.76
5.49	0.34	0.54	1.59
5.52	0.34	0.54	1.59
5.99	0.34	0.54	1.59
6.12	0.34	0.68	2.00
6.61	0.34	0.6	1.76
6.75	0.34	0.48	1.41
7.07	0.34	0.57	1.68
7.18	0.34	0.66	1.94
7.67	0.34	0.68	2.00
8.36	0.33	0.64	1.94
9.2	0.33	0.63	1.91

Table 5.1 Static and Dynamic Critical Tram Data

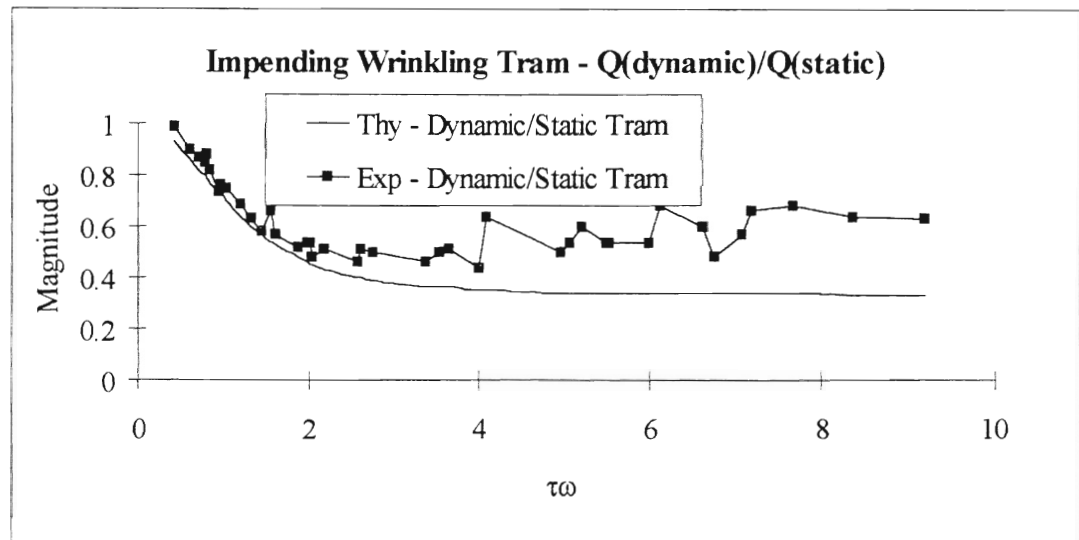


Figure 5.2 Impending Wrinkling Tram (Dynamic/Static ratio)

Figure 5.2 illustrates that, theoretically, the dynamic critical tram is one third the value of the static critical tram at high $\tau\omega$ for equivalent tram angles, web line parameters, and web properties. Figure 5.2 also illustrates how experimental data varies from theoretical data with increasing $\tau\omega$.

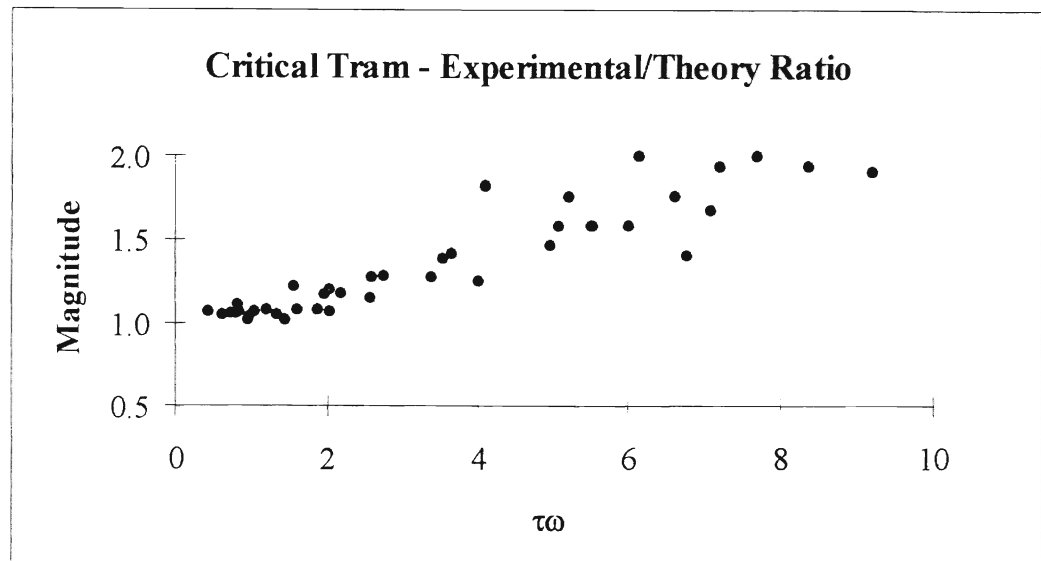


Figure 5.3 Critical Tram - Experimental/Theory Ratio

Figure 5.3 illustrates how the experimental to theoretical ratio varies, as $\tau\omega$ increases. At low $\tau\omega$ values, equivalent to static wrinkling, experimental and theoretical values approach the same magnitude. Conversely, as $\tau\omega$ increases, the experimental to theoretical ratio increases to a magnitude near 2. In other words, nearly twice the tram predicted by theory is necessary to wrinkle the web at large $\tau\omega$.

CHAPTER VI

Discussion

At this point, we have found that the static wrinkling model presented in Chapter 3 is inadequate to describe dynamic wrinkling as identified by experiments. The following analyses were performed to investigate parameters which may or may not need to be accounted for in the dynamic wrinkling model.

6.1 Analysis of Dynamic Stress State in Web

When considering high $\tau\omega$ values, the lateral displacement amplitude ratio approaches zero and the in-plane bending moment at the tram roller increases with increasing tram. At high $\tau\omega$, due to small lateral displacement, the web is accurately modeled as a cantilevered - pinned beam with an imposing moment acting on the pinned end as illustrated in Figure 6.1.

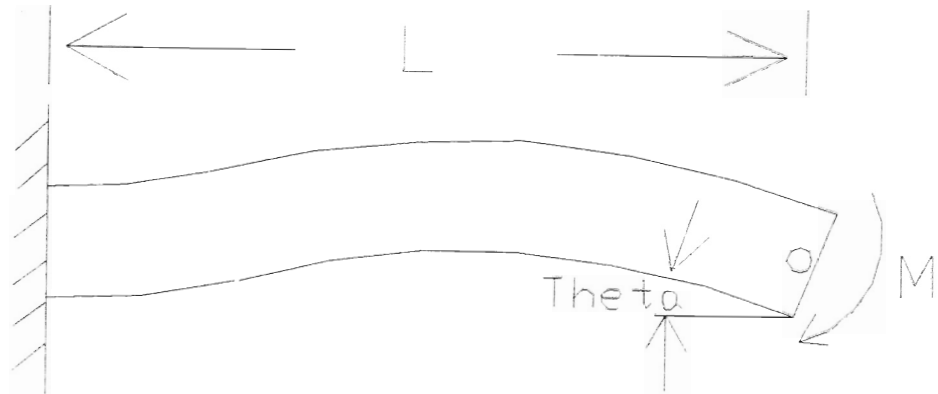


Figure 6.1 Cantilevered - Pinned Beam

For this pinned-cantilevered beam, the moment necessary to cause the rotation angle θ is given by equation (6.1).

$$M = \frac{4EI\theta}{L} \quad (6.1)$$

Similarly, the shear force due to the rotation angle θ is written as:

$$N = \frac{6EI\theta}{L^2} \quad (6.2)$$

Note that the shear force represented by equation (6.2) is 3 times the magnitude of the shear for the static case represented by equation (1.2). These elementary beam models of shear and moment agree with Shelton's frequency response derivation [1] for large $\tau\omega$.

More exact than (6.1), the moment in the web for high frequency response is represented by equation (6.3).

$$M_L = -\frac{TL\theta_L}{(KL)^2} f_2 \quad (6.3)$$

Similarly, approximating for small KL , equation (6.3) is written as:

$$M_L = -4\frac{TL\theta_L}{(KL)^2} \quad (6.4)$$

Applying elementary beam analysis to the web, the MD stress state is now described for large $\tau\omega$ conditions. A simple beam loaded with a bending moment on the end will have a linearly varying stress distribution. This stress distribution varies as described by equation (6.5).

$$\sigma_x = \frac{Mc}{I} \quad (6.5)$$

Hence, for a tram displacement at high $\tau\omega$, the stress distribution in the web immediately preceding the roller is graphically illustrated with Figure 6.2.

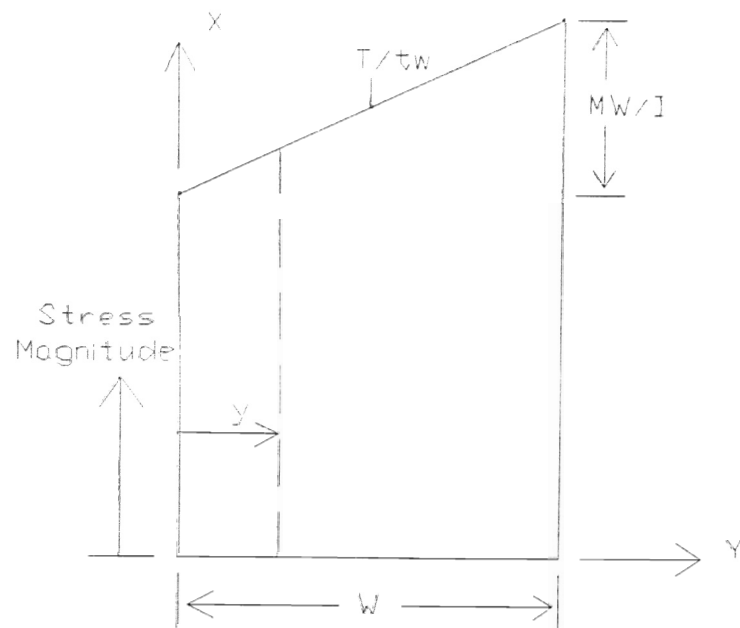


Figure 6.2 Web stress distribution drawing - dynamic conditions.

The maximum and minimum stress magnitude at the web edges increases and decreases, respectively, with M . Thus, for small or negligible tram displacements, the bending moment approaches zero, leading to a constant stress distribution.

6.1.1 Effect of Varying Stress Distribution on Critical Compressive Stress

Using a critical tram displacement for high $\tau\omega$, $q = 0.033$ in., to calculate the maximum bending moment within the web results in $M = 3.973$ lb-in. Substituting $M = 3.973$ in-lb, $c = 3$ in., and $I = 0.00864$ in⁴, results in a MD stress increase of 1380 psi on the high stress edge and a decrease of 1380 psi on the low stress edge. All experiments were performed at 9 lb. MD tension which results in an average MD stress of 3125 psi.

Thus, the change in stress due to bending is plus and minus 45% on the high and low stress edge, respectively. Observation of Shelton's simplified critical stress, equation (3.9), shows that the critical stress is proportional to the square root of the MD stress. From this, we can conclude that the critical compressive stress on the edge increases no more than the square root of $(1 + 0.45)$ times the average critical compressive stress in the center of the web. Similarly, the critical compressive stress on the low stress edge decreases no less than the square root of $(1 - 0.45)$ times the average critical compressive stress in the center of the web.

However, by observing wrinkling experiments, it is obvious that a wrinkle occurs at approximately 40 % of the web width into the web or, 10 % of the web width from the center of the web. At this point on the web, the change in MD stress due to bending is only plus and minus 9 % of the average MD stress. Thus, the change in critical compressive stress, due to the 9 % change in MD stress, is 1.04 times the average critical compressive for the high stress side, and 0.96 times the average critical compressive stress for the low stress side. This change in critical compressive stress is insignificant and will not be considered further in the final formulation of the dynamic wrinkling algorithm.

6.1.2 Effect of Varying Stress Distribution on Traction Capacity

The traction capacity of a web is defined as the maximum amount of lateral force per unit length within the web required to cause web slippage upon a roller. The traction

capacity equation is documented in [5] for uniform web stress and is shown below in equation (6.5).

$$f_{\mu} = \frac{T}{wR} \mu y \quad (6.5)$$

Where y is the distance from the web edge to the point of interest in inches.

For many practical static wrinkling and traction applications, the tension immediately preceding the tram roller of interest approaches a constant value. In the case of a constant tension distribution the traction capacity increases linearly from the web edge to its maximum value at the center of the web, and then decreases linearly beyond the web center to the other edge. For the purpose of developing a dynamic wrinkling algorithm, it is important to understand how the traction capacity varies with the bending moment. This is important because, at any instant, one side of the web has a lower stress magnitude than the opposite side of the web, therefore causing a nonlinear variance of traction capacity across the web width.

By understanding how the traction capacity varies with the web width, one can determine if either side of the web, particularly the lower stress side, has sufficient traction to support a wrinkle. The traction decreases on the lower stress side; on the other hand, the MD stress decreases, thus requiring a lower buckling stress. However, it was concluded in section 6.1.1 that the change in critical compressive stress due to the bending moment is an insignificant factor in the development of the wrinkling algorithm and will no longer be considered.

Referring to the web MD stress distribution graph in Figure 6.2, a relationship for tension variance with respect to web width is derived, as is needed for equation (6.5).

This expression for tension per unit width is then substituted into equation (6.5) to get an equivalent expression of web traction capacity, as a function of the bending moment. The equivalent stress represented as a function of y is:

$$\sigma_x(y) = \frac{T}{tw} + \frac{M}{I} \left(y - \frac{w}{2} \right) \quad (6.6)$$

The traction capacity equation (6.5) requires the tension per unit width (T/w). Thus, multiplying (6.6) by the web thickness, substituting $I = (1/12)tw^3$, and dividing by R, results in the equivalent pressure per unit width between the web and roller as shown in equation (6.7).

$$P = \left(\frac{T}{wR} \right)_{EQ} = \frac{\sigma(y)t}{R} = \frac{T}{wR} + \frac{12M}{w^3R} \left(y - \frac{w}{2} \right) \quad (6.7)$$

Integrating (6.7), with respect to y, yields the modified traction capacity equation for high $\tau\omega$, taut, center pivoted, planar webs and is shown in equation (6.8).

$$\frac{F}{s} = \left[\frac{Ty}{w} + \frac{12M}{w^3} \left(\frac{y^2}{2} - \frac{yw}{2} \right) \right] \frac{\mu}{R} \quad (6.8)$$

However, the traction capacity is defined as the minimum of the capacity of either side of the point of interest y , to resist slippage as shown in Figure 6.2. For this reason we must derive the force per unit length expression assuming the origin begins at the opposite side of the web. However, the stress must still be tensile, or positive, on the right hand edge of the web. This is achieved by substituting $(w/2 - y)$ for $(y - w/2)$ into equation (6.7) and integrating as before. After integrating, the expression of force per unit length with the origin at the high stress edge is equation (6.9).

$$\frac{F}{s} = \left[\frac{Ty}{w} + \frac{12M}{w^3} \left(-\frac{y^2}{2} + \frac{yw}{2} \right) \right] \frac{\mu}{R} \quad (6.9)$$

Hence, the true traction capacity over the full width of the web at any distance y from the edge is the minimum of equations (6.8) and (6.9) with y varying from 0 to w .

Now that the tension and traction capacity expressions are established, the traction coefficient, μ , must be considered because it is also a function of tension and air entrainment. The coefficient of traction is directly dependent on the air film thickness, h_o . Knox-Sweeney [8] developed a relation describing h_o as a function of air properties and web line parameters as shown in equation (6.10).

$$h_o = 0.65R \left[\frac{12\nu V}{T} \right]^{\frac{2}{3}} \quad (6.10)$$

Multiply equation (6.7) by the wrap distance, s , to obtain the web tension as a function of y , and substitute $F(y)$ into equation (6.10) to get the resulting Knox-Sweeney air film equation accounting for the tension variation across the web width.

Solely for the purpose of determining a worst case scenario, a maximum moment encountered during high frequency conditions is used in the calculation because this is when insufficient traction problems would occur. After substituting $T(y)$ and a maximum moment of 3.97 lb-in., into equation (6.10), h_o is found to vary from $3.22 \text{ E } -5$ in. on the low stress edge to $1.71 \text{ E } -5$ in. on the high stress edge. Previous experimental air film height data gives a traction coefficient corresponding to h_{\max} and h_{\min} of 0.16 to 0.25, respectively. Here 0.16 corresponds to the low stress edge and 0.25 corresponds to the high stress edge. v is assumed to vary linearly from $y = 0$ to $y = w$. Incorporating these numbers for the traction coefficient and the expression for the lateral tension variation into equation (6.8) and (6.9), and plotting the minimum of both equations for $y = 0$ to $y = w$ results in the following graph.

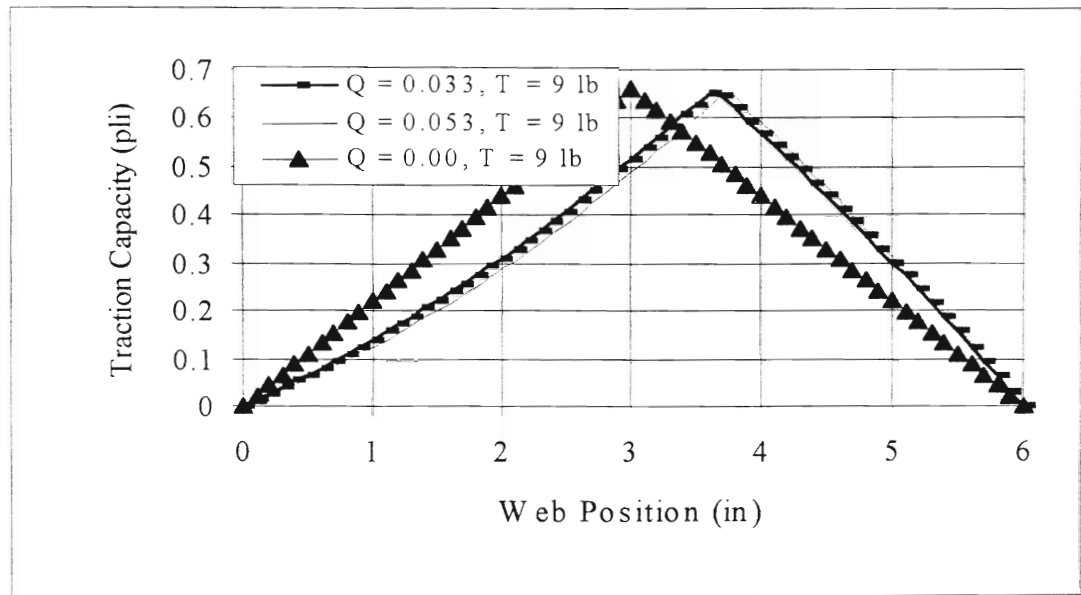


Figure 6.3 Traction Capacity Variance - Dynamic Conditions

Figure 6.3 represents the traction capacity at high $\tau\omega$ and for several different tram errors. The curve for $Q = 0.0$ in. is equivalent to static conditions, and note that this traction capacity curve is a linear response. For comparison purposes, two different tram displacement traction capacities are plotted. $Q = 0.033$ in. is a common experimental high $\tau\omega$ critical tram. The traction capacity for $Q = 0.053$ in. is plotted to illustrate how traction capacity varies with tram.

To determine whether the change in traction capacity due to the bending moment has any effect on wrinkling, calculations are made to determine the lateral force per unit width necessary to buckle the web. When this force is known, one can determine the percentage of web width necessary to support a wrinkle. This is calculated with the equation documented in [5] shown in equation (6.11).

$$f_{y,cr} = -0.605E \frac{t^2}{R} \quad (6.11)$$

Where $f_{y,cr}$ is the internal force per unit length of the web necessary to cause web buckling. Thus, plotting $f_{y,cr}$ on the traction capacity graph and noting at what web edge displacement the equations are equal, gives the distance into the web where sufficient traction exists to support a wrinkle. This is illustrated below in Figure 6.4.

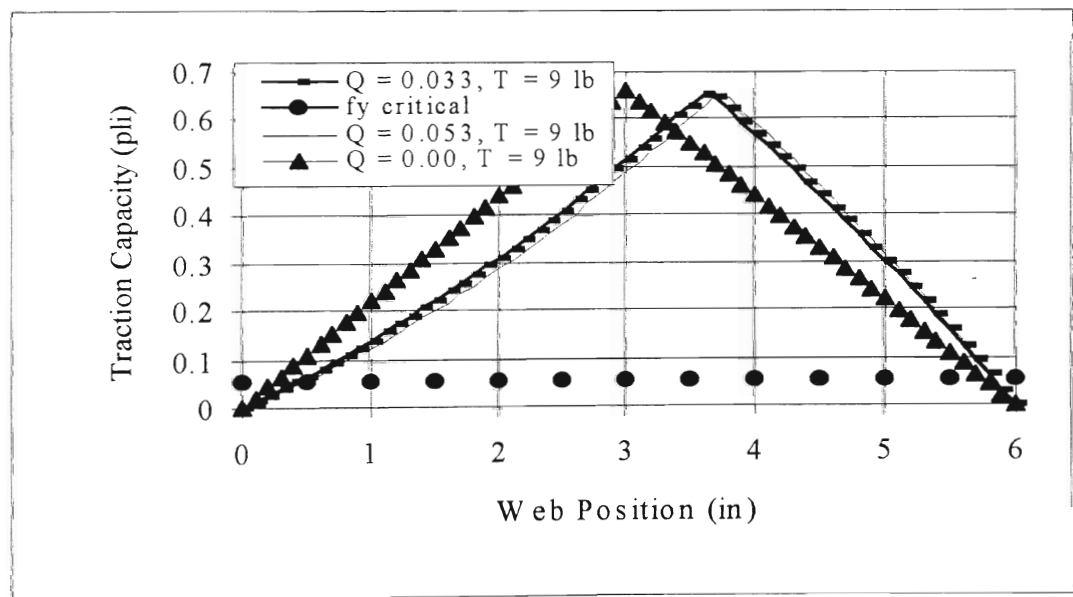


Figure 6.4 Web Traction Capacity Versus the Load Necessary to Buckle the Web

Shown in Figure 6.4 is the distance from either web edge where sufficient traction exists to support a wrinkle. From the low stress edge and high stress edge, only less than

one-half inch of web is needed to provide sufficient traction to sustain a wrinkle.

Experimental observation shows that, at high $\tau\omega$, the wrinkle forms approximately 40% inward from the high stress edge. Due to the bending moment, the traction capacity is decreased on the low stress edge of the web, below the traction capacity for a uniform stress condition. In any case, the traction capacity is much in excess of the load required to retain the web in a wrinkled condition as the web passes over a roller. Note that for v changing from 0.16 to 0.25 has negligible effect on the ability of the web to support a wrinkle. Thus, the traction capacity variation across the web width due to the bending moment is not a significant factor affecting the discrepancy between theoretical predictions and experimental results of critical tram error.

6.2 Dynamic Wrinkling Algorithm

Many web line systems use a pivoting or laterally traversing tram roller to laterally position the web. Many of the web guide systems give an output tram velocity proportional to the input signal. If a discontinuous web edge exists due to a splice or manufacturing problem, then the web edge sensor sees a step input. This step input, in turn, causes a high tram velocity response. If the combined tram velocity and tram displacement is large enough, then large dynamic shears are produced leading to web failure, provided that sufficient traction exists to support a wrinkle. Web failure results in a decrease in product quality and lower customer satisfaction.

The economic importance of web degradation varies between different products. For example, a scratch or wrinkle in a newspaper may be much less costly than a scratch or wrinkle on a sample of pressure sensitive film. Hence, this constitutes the development of a dynamic wrinkling algorithm that predicts web failure as a function of web material properties, web line properties, tram rate and tram displacement. Accurate prediction of web failure allows one to alter system parameters so as to avoid wrinkling, thus resulting in improved product quality, less wasted resources, and increased customer satisfaction.

The theoretical predictions of lateral displacement amplitude ratio and phase lag were confirmed as recorded in Chapter 5. The experimental confirmation led to confidence in the magnitude and phase lag of shear existing within the web as described by equation (2.2.16). The fact that the experimental critical tram increases to twice the theoretical predicted critical tram at high $\tau\omega$, leads one to believe that the web wrinkles due to an RMS value of shear. However, two obvious experimental observations show that more is involved with wrinkling than just the RMS shear value. First, the experimental critical tram merges with theory at low $\tau\omega$ as depicted in Figure 5.3. This is important because if the web wrinkled due to an RMS shear, and if the peak shear was equal to the critical shear, then a much lower critical tram would be necessary than predicted by theory. Second, at medium and low values of $\tau\omega$, the RMS shear is less than the critical shear and the peak shear barely exceeds the critical shear, yet the web wrinkles. These two facts lead to the conclusion that the web wrinkles according to a time variance of shear as discussed in section 6.2.1.

6.2.1 Time Variance of Shear

It is considered that the web will wrinkle if the following two conditions are true:

- 1) the magnitude of shear in the web is greater than the critical shear.
- 2) this magnitude of shear does not drop below the critical shear for the period of time required for a wrinkle to transgress the roller.

For the first criterion, the magnitude of shear in the web is determined from the dynamic shear equation, equation (2.2.16), and then equation (3.11) is used to calculate the critical shear. The second criterion is checked by comparing the amount of time the web is in contact with the roller with the amount of time that the shear exceeds the critical shear. Equations are derived below which enable one to easily calculate conditions to check criterion two.

$$\sin(t_1) = \frac{N_{cr}}{N_{peak}} \quad (6.1)$$

Solving for t_1 yields:

$$t_1 = \sin^{-1}\left(\frac{N_{cr}}{N_{peak}}\right) \quad (6.2)$$

Where t_1 represents the beginning point of where the shear magnitude equals the critical shear. Similarly, t_2 is the point at which the shear magnitude drops below the critical shear. For a sine wave, the slope magnitude is equal but is opposite in sign. Thus,

$$\frac{d}{dt} \sin(t_1) = -\frac{d}{dt} \sin(t_2) \quad (6.3)$$

Or,

$$\cos(t_1) = -\cos(t_2) \quad (6.4)$$

Solving for t_2 yields equation (6.5).

$$t_2 = \cos^{-1}[-\cos(t_1)] \quad (6.5)$$

t_1 and t_2 are not units of time; however, $t_2 - t_1$ represents a part of the period T . Thus, equation (6.6) shown below enables one to calculate the length of time that a shear force stays in the web before dropping below N_{cr} .

$$\frac{t_2 - t_1}{2\pi} T \quad (6.6)$$

However, $\omega T = 2\pi$, so equation (6.6) simplifies into equation (6.7).

However, $\omega T = 2\pi$, so equation (6.6) simplifies into equation (6.7).

$$\frac{t_2 - t_1}{\omega} \quad (6.7)$$

A simplified way of calculating equation (6.7) is shown in equation (6.8).

$$\frac{t_2 - t_1}{\omega} = \frac{2}{\omega} \cos^{-1} \left[\frac{N_{cr}}{N_{peak}} \right] \quad (6.8)$$

The time a particular point of the web spends on the roller for a given wrap angle is:

$$\tau_r = \frac{R\theta}{V} \quad (6.9)$$

Finally, the failure criterion is summarized as follows. The web will wrinkle if:

1) The peak shear is greater than the critical shear, and

$$2) \frac{2}{\omega} \cos^{-1} \left[\frac{N_{cr}}{N_{peak}} \right] \geq \frac{\theta}{V} R \quad (6.10)$$

A table of experimental wrinkle data along with the 1) and 2) wrinkle criteria is shown below.

$\tau\omega$	N - eqn. (2.2.16)	V (fpm)	ω (rad/s)	{1} τ_r	{2} $2 \cdot \omega \cdot \text{Acos}(N_{cr}/N_{peak})$
0.43	0.23	98.00	0.468	0.120	#NUM!
0.61	0.22	91.00	0.617	0.129	#NUM!
0.72	0.23	80.00	0.640	0.147	#NUM!
0.78	0.23	80.00	0.693	0.147	#NUM!
0.8	0.24	69.00	0.613	0.171	0.298
0.84	0.23	50.00	0.467	0.236	#NUM!
0.95	0.21	58.00	0.612	0.203	#NUM!
0.96	0.22	60.00	0.640	0.196	#NUM!
1.03	0.23	60.00	0.687	0.196	#NUM!
1.2	0.23	87.00	1.160	0.135	#NUM!
1.32	0.22	42.00	0.616	0.280	#NUM!
1.44	0.22	40.00	0.640	0.295	#NUM!
1.55	0.26	40.00	0.689	0.295	1.175
1.61	0.23	65.00	1.163	0.181	#NUM!
1.88	0.23	95.00	1.984	0.124	#NUM!
1.97	0.25	53.00	1.160	0.222	0.513
2.02	0.25	90.00	2.020	0.131	0.295
2.03	0.22	28.00	0.632	0.421	#NUM!
2.18	0.25	82.00	1.986	0.144	0.300
2.57	0.24	101.00	2.884	0.117	0.063
2.6	0.27	70.00	2.022	0.168	0.479
2.75	0.27	90.00	2.750	0.131	0.352
3.37	0.27	53.00	1.985	0.222	0.488
3.53	0.3	70.00	2.746	0.168	0.473
3.64	0.3	50.00	2.022	0.236	0.642
4	0.27	65.00	2.889	0.181	0.335
4.09	0.39	31.00	1.409	0.380	1.294
4.96	0.31	50.00	2.756	0.236	0.501
5.07	0.34	25.00	1.408	0.471	1.124
5.2	0.37	35.00	2.022	0.337	0.859
5.49	0.34	24.00	1.464	0.491	1.081
5.52	0.34	23.00	1.411	0.512	1.122
5.99	0.34	22.00	1.464	0.535	1.081
6.12	0.43	27.00	1.836	0.436	1.069
6.61	0.38	25.00	1.836	0.471	0.970
6.75	0.31	20.00	1.500	0.589	0.921
7.07	0.36	35.00	2.749	0.337	0.615
7.18	0.42	23.00	1.835	0.512	1.052
7.67	0.43	24.00	2.045	0.491	0.960
8.36	0.41	22.00	2.044	0.535	0.928
9.2	0.4	20.00	2.044	0.589	0.910

Table 6.1 Experimental Shear and Time Variance Data

The entries in Figure 6.5 labeled #NUM! are results obtained when an imaginary number from a calculation is encountered. These imaginary numbers are caused by taking the inverse cosine of a number greater than 1. More specifically, for these cases, N_{peak} was less than N_{cr} , causing $\text{Acos}(N_{\text{cr}}/N_{\text{peak}})$ to be imaginary. This is due to discrepancies while taking experimental data. Theoretically N_{peak} should be greater than N_{cr} for a wrinkle to occur.

A plot comparing τ_r with $2/w * \text{Acos}(N_{\text{cr}}/N_{\text{peak}})$ is shown below in Figure 6.6.

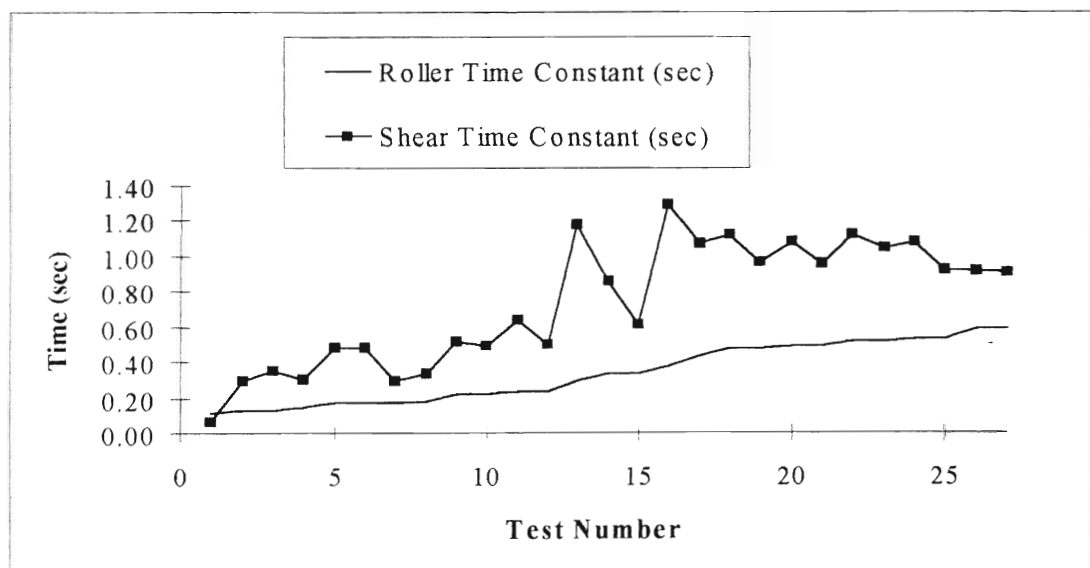


Figure 6.5 Plot of Wrinkle Criteria

By comparing columns {1} and {2}, it is evident that column {2} is approximately 2 times column {1}. Theoretically, according to equation (6.10), columns {1} and {2} should be equal at the point of wrinkle. From these data, considering only a 90 degree wrap angle, one may conclude that the shear needs to exist for the time necessary for a

necessary for a point on the web to move across one-half of the roller wrap length, $R\theta$, to produce a permanent wrinkle. A plot of this empirically modified wrinkle criteria is shown below in Figure 6.6.

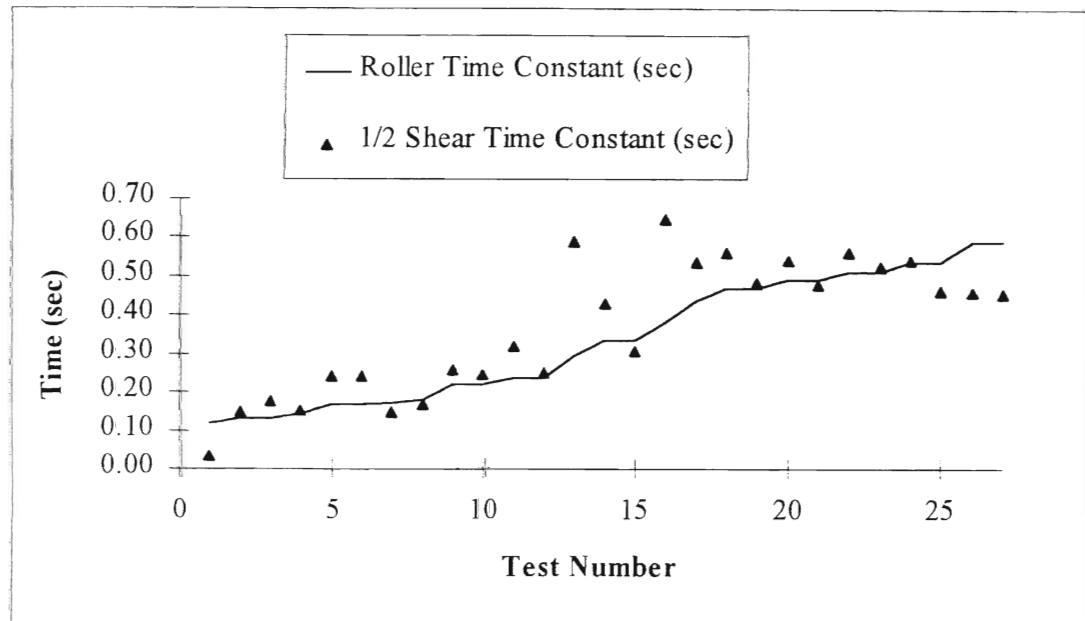


Figure 6.6 Empirically Modified Wrinkle Criteria

Assuming the shear needs to exist for only one half of the roller wrap length is valid for a 90 degree wrap angle. However, this empirically modified wrinkle criteria will most likely fail for any other wrap angles. Future research should include wrinkle experiments at varying degrees of wrap angle.

CHAPTER VII

Conclusions

7.1 Overview

Development of the dynamic wrinkling algorithm is important for the improvement of industrial web line systems. With the exception of non parallel rollers, many wrinkles occur due to over steering the web either in the web line or on the rewind. The static wrinkling algorithm agrees well with experimental data and is important for non parallel rollers, which encompasses many wrinkling problems. However, the dynamic wrinkling algorithm covers many other wrinkling problems such as web guiding systems.

The dynamic wrinkling criteria can be stated as follows. A wrinkle will progress into a permanent deformation in the web if the following two criteria are met.

1) The peak shear is greater than the critical shear, and

$$2) \frac{1}{\omega} \cos^{-1} \left[\frac{N_{cr}}{N_{peak}} \right] \geq \frac{\theta}{V} R$$

The shear force is cyclic with a frequency equal to that of the tram frequency. This means that the web “sees” peak values of shear changing direction twice per period, and while changing directions the shear force passes through zero. The shear force that equation (2.2.16) predicts is the peak shear that the web experiences. However, it is apparent that the web reacts to the root mean square value of shear, not different than how an electric appliance operates on the RMS value of the input voltage. In addition to the web wrinkling from an RMS value of shear, this RMS shear must exist long enough for a wrinkle to traverse the roller as discussed in Chapter 6.1.1.

The failure criteria listed above in 1) and 2) for regime I, taut, planar have been experimentally verified at the Oklahoma State University Web Handling Research Center. Accurate prediction of web failure, while subject to dynamic conditions, requires having sufficient traction between the web and roller, which usually implies having low web velocities, accurate web tension, accurate tram error, and accurate measurement of tram frequency and period. These conditions are not always achievable in common industrial production web lines. However, this research brings forth a knowledge base about dynamic wrinkling that is essential for further wrinkling research.

7.2 Future Work

Future work expanding the wrinkling research should contain work with lateral displacement, and off center pivot tram rollers. These two types of steering systems encompass a large part of the web guide systems employed in industry. This should also

encompass the regime I and regime II wrinkling areas. Regime II is a separate field of wrinkling where traction between the web and roller is not large enough to prevent web slippage. Much of the aforementioned theory fails for regime II wrinkling.

REFERENCES

1. Shelton, J. J., June 1994.
2. Shelton, J. J., "Lateral Dynamics of a Real Moving Web." Thesis, Department of Mechanical and Aerospace Engineering, Oklahoma State University, 1968.
3. Reid, K. N., and Shelton, J. J., "Lateral Dynamics of a Real Moving Web." Journal of Dynamic Systems, Measurement, and Control, September, 1971.
4. Quan, Wen, "Web Wrinkling Prediction and Failure Analysis." Thesis, , Department of Mechanical and Aerospace Engineering, Oklahoma State University, 1993.
5. Shelton, J., J., "Buckling of Webs From Lateral Compressive Forces." Proceedings of the Second International Conference on Web Handling, June 6-9, 1993, Oklahoma State University, Stillwater, OK.
6. Timoshenko, S.P. and Gere, J.M., "Theory of Elastic Stability," McGraw-Hill Book Company, New York, Second Edition, 1961.
7. Gehlbach, L.S., Kedl, D.M., and Good, J. K., "Predicting Shear Wrinkles in Web Spans," TAPPI Journal, August, 1989.
8. Knox, K.L. and Sweeney, T.L., "Fluid Effects Associated with Web Handling," Industrial Engineering Chemical Process Design Development, Vol 10, No. 2, 1971, pp.201-205.

VITA

Jason Mitchell

Candidate for the Degree of

Master of Science

Thesis: PREDICTION AND FAILURE ANALYSIS OF WEB WRINKLING

Major Field: Mechanical Engineering

Biographical:

Personal Data: Born in Nashville, Tennessee, on September 27, 1970, the son of Alan and Diane Mitchell.

Education: Graduated from Collinsville High School, Collinsville, Oklahoma in May 1988; received a Bachelor of Science degree in Mechanical Engineering from Oklahoma State University in May 1993. Completed the requirements for the Master of Science degree with a major in Mechanical Engineering in May 1995.

Experience: Employed as an engineer assistant for Reda Pump, Inc., and Enardo Manufacturing, Co., in the summers of 1991 and 1992, respectively; employed by Oklahoma State University as a graduate research assistant, June 1993 to December 1994.

Professional Memberships: American Society of Mechanical Engineers, student member.